Physics Letters B 737 (2014) 357–365

Contents lists available at ScienceDirect

Physics Letters B

www.elsevier.com/locate/physletb

Measurement of the differential $\gamma + 2b$-jet cross section and the ratio $\sigma(\gamma + 2b\text{-jets})/\sigma(\gamma + b\text{-jet})$ in $p\bar{p}$ collisions at $\sqrt{s} = 1.96$ TeV

D0 Collaboration

V.M. Abazov [af], B. Abbott [bp], B.S. Acharya [z], M. Adams [au], T. Adams [as], J.P. Agnew [ap], G.D. Alexeev [af], G. Alkhazov [aj], A. Alton [be,1], A. Askew [as], S. Atkins [bc], K. Augsten [g], C. Avila [e], F. Badaud [j], L. Bagby [at], B. Baldin [at], D.V. Bandurin [bv], S. Banerjee [z], E. Barberis [bd], P. Baringer [bb], J.F. Bartlett [at], U. Bassler [o], V. Bazterra [au], A. Bean [bb], M. Begalli [b], L. Bellantoni [at], S.B. Beri [x], G. Bernardi [n], R. Bernhard [t], I. Bertram [an], M. Besançon [o], R. Beuselinck [ao], P.C. Bhat [at], S. Bhatia [bg], V. Bhatnagar [x], G. Blazey [av], S. Blessing [as], K. Bloom [bh], A. Boehnlein [at], D. Boline [bm], E.E. Boos [ah], G. Borissov [an], M. Borysova [am,12], A. Brandt [bs], O. Brandt [u], R. Brock [bf], A. Bross [at], D. Brown [n], X.B. Bu [at], M. Buehler [at], V. Buescher [v], V. Bunichev [ah], S. Burdin [an,2], C.P. Buszello [al], E. Camacho-Pérez [ac], B.C.K. Casey [at], H. Castilla-Valdez [ac], S. Caughron [bf], S. Chakrabarti [bm], K.M. Chan [az], A. Chandra [bu], E. Chapon [o], G. Chen [bb], S.W. Cho [ab], S. Choi [ab], B. Choudhary [y], S. Cihangir [at], D. Claes [bh], J. Clutter [bb], M. Cooke [at,11], W.E. Cooper [at], M. Corcoran [bu], F. Couderc [o], M.-C. Cousinou [l], D. Cutts [br], A. Das [aq], G. Davies [ao], S.J. de Jong [ad,ae], E. De La Cruz-Burelo [ac], F. Déliot [o], R. Demina [bl], D. Denisov [at], S.P. Denisov [ai], S. Desai [at], C. Deterre [u,3], K. DeVaughan [bh], H.T. Diehl [at], M. Diesburg [at], P.F. Ding [ap], A. Dominguez [bh], A. Dubey [y], L.V. Dudko [ah], A. Duperrin [l], S. Dutt [x], M. Eads [av], D. Edmunds [bf], J. Ellison [ar], V.D. Elvira [at], Y. Enari [n], H. Evans [ax], V.N. Evdokimov [ai], A. Fauré [o], L. Feng [av], T. Ferbel [bl], F. Fiedler [v], F. Filthaut [ad,ae], W. Fisher [bf], H.E. Fisk [at], M. Fortner [av], H. Fox [an], S. Fuess [at], P.H. Garbincius [at], A. Garcia-Bellido [bl], J.A. García-González [ac], V. Gavrilov [ag], W. Geng [l,bf], C.E. Gerber [au], Y. Gershtein [bi], G. Ginther [at,bl], O. Gogota [am], G. Golovanov [af], P.D. Grannis [bm], S. Greder [p], H. Greenlee [at], G. Grenier [q,r], Ph. Gris [j], J.-F. Grivaz [m], A. Grohsjean [o,3], S. Grünendahl [at], M.W. Grünewald [aa], T. Guillemin [m], G. Gutierrez [at], P. Gutierrez [bp], J. Haley [bq], L. Han [d], K. Harder [ap], A. Harel [bl], J.M. Hauptman [ba], J. Hays [ao], T. Head [ap], T. Hebbeker [s], D. Hedin [av], H. Hegab [bq], A.P. Heinson [ar], U. Heintz [br], C. Hensel [a], I. Heredia-De La Cruz [ac,4], K. Herner [at], G. Hesketh [ap,6], M.D. Hildreth [az], R. Hirosky [bv], T. Hoang [as], J.D. Hobbs [bm], B. Hoeneisen [i], J. Hogan [bu], M. Hohlfeld [v], J.L. Holzbauer [bg], I. Howley [bs], Z. Hubacek [g,o], V. Hynek [g], I. Iashvili [bk], Y. Ilchenko [bt], R. Illingworth [at], A.S. Ito [at], S. Jabeen [at,13], M. Jaffré [m], A. Jayasinghe [bp], M.S. Jeong [ab], R. Jesik [ao], P. Jiang [d], K. Johns [aq], E. Johnson [bf], M. Johnson [at], A. Jonckheere [at], P. Jonsson [ao], J. Joshi [ar], A.W. Jung [at], A. Juste [ak], E. Kajfasz [l], D. Karmanov [ah], I. Katsanos [bh], M. Kaur [x], R. Kehoe [bt], S. Kermiche [l], N. Khalatyan [at], A. Khanov [bq], A. Kharchilava [bk], Y.N. Kharzheev [af], I. Kiselevich [ag], J.M. Kohli [x], A.V. Kozelov [ai], J. Kraus [bg], A. Kumar [bk], A. Kupco [h], T. Kurča [q,r], V.A. Kuzmin [ah], S. Lammers [ax], P. Lebrun [q,r], H.S. Lee [ab], S.W. Lee [ba], W.M. Lee [at], X. Lei [aq], J. Lellouch [n], D. Li [n], H. Li [bv], L. Li [ar], Q.Z. Li [at], J.K. Lim [ab], D. Lincoln [at], J. Linnemann [bf], V.V. Lipaev [ai], R. Lipton [at], H. Liu [bt], Y. Liu [d], A. Lobodenko [aj], M. Lokajicek [h], R. Lopes de Sa [bm], R. Luna-Garcia [ac,7], A.L. Lyon [at], A.K.A. Maciel [a], R. Madar [t], R. Magaña-Villalba [ac], S. Malik [bh], V.L. Malyshev [af], J. Mansour [u], J. Martínez-Ortega [ac],

http://dx.doi.org/10.1016/j.physletb.2014.09.007

R. McCarthy [bm], C.L. McGivern [ap], M.M. Meijer [ad,ae], A. Melnitchouk [at], D. Menezes [av], P.G. Mercadante [c], M. Merkin [ah], A. Meyer [s], J. Meyer [u,9], F. Miconi [p], N.K. Mondal [z], M. Mulhearn [bv], E. Nagy [l], M. Narain [br], R. Nayyar [aq], H.A. Neal [be], J.P. Negret [e], P. Neustroev [aj], H.T. Nguyen [bv], T. Nunnemann [w], J. Orduna [bu], N. Osman [l], J. Osta [az], A. Pal [bs], N. Parashar [ay], V. Parihar [br], S.K. Park [ab], R. Partridge [br,5], N. Parua [ax], A. Patwa [bn,10], B. Penning [at], M. Perfilov [ah], Y. Peters [ap], K. Petridis [ap], G. Petrillo [bl], P. Pétroff [m], M.-A. Pleier [bn], V.M. Podstavkov [at], A.V. Popov [ai], M. Prewitt [bu], D. Price [ap], N. Prokopenko [ai], J. Qian [be], A. Quadt [u], B. Quinn [bg], P.N. Ratoff [an], I. Razumov [ai], I. Ripp-Baudot [p], F. Rizatdinova [bq], M. Rominsky [at], A. Ross [an], C. Royon [o], P. Rubinov [at], R. Ruchti [az], G. Sajot [k], A. Sánchez-Hernández [ac], M.P. Sanders [w], A.S. Santos [a,8], G. Savage [at], M. Savitskyi [am], L. Sawyer [bc], T. Scanlon [ao], R.D. Schamberger [bm], Y. Scheglov [aj], H. Schellman [aw], C. Schwanenberger [ap], R. Schwienhorst [bf], J. Sekaric [bb], H. Severini [bp], E. Shabalina [u], V. Shary [o], S. Shaw [ap], A.A. Shchukin [ai], V. Simak [g], P. Skubic [bp], P. Slattery [bl], D. Smirnov [az], G.R. Snow [bh], J. Snow [bo], S. Snyder [bn], S. Söldner-Rembold [ap], L. Sonnenschein [s], K. Soustruznik [f], J. Stark [k], D.A. Stoyanova [ai], M. Strauss [bp], L. Suter [ap], P. Svoisky [bp], M. Titov [o], V.V. Tokmenin [af], Y.-T. Tsai [bl], D. Tsybychev [bm], B. Tuchming [o], C. Tully [bj], L. Uvarov [aj], S. Uvarov [aj], S. Uzunyan [av], R. Van Kooten [ax], W.M. van Leeuwen [ad], N. Varelas [au], E.W. Varnes [aq], I.A. Vasilyev [ai], A.Y. Verkheev [af], L.S. Vertogradov [af], M. Verzocchi [at], M. Vesterinen [ap], D. Vilanova [o], P. Vokac [g], H.D. Wahl [as], M.H.L.S. Wang [at], J. Warchol [az], G. Watts [bw], M. Wayne [az], J. Weichert [v], L. Welty-Rieger [aw], M.R.J. Williams [ax], G.W. Wilson [bb], M. Wobisch [bc], D.R. Wood [bd], T.R. Wyatt [ap], Y. Xie [at], R. Yamada [at], S. Yang [d], T. Yasuda [at], Y.A. Yatsunenko [af], W. Ye [bm], Z. Ye [at], H. Yin [at], K. Yip [bn], S.W. Youn [at], J.M. Yu [be], J. Zennamo [bk], T.G. Zhao [ap], B. Zhou [be], J. Zhu [be], M. Zielinski [bl], D. Zieminska [ax], L. Zivkovic [n]

[a] *LAFEX, Centro Brasileiro de Pesquisas Físicas, Rio de Janeiro, Brazil*
[b] *Universidade do Estado do Rio de Janeiro, Rio de Janeiro, Brazil*
[c] *Universidade Federal do ABC, Santo André, Brazil*
[d] *University of Science and Technology of China, Hefei, People's Republic of China*
[e] *Universidad de los Andes, Bogotá, Colombia*
[f] *Charles University, Faculty of Mathematics and Physics, Center for Particle Physics, Prague, Czech Republic*
[g] *Czech Technical University in Prague, Prague, Czech Republic*
[h] *Institute of Physics, Academy of Sciences of the Czech Republic, Prague, Czech Republic*
[i] *Universidad San Francisco de Quito, Quito, Ecuador*
[j] *LPC, Université Blaise Pascal, CNRS/IN2P3, Clermont, France*
[k] *LPSC, Université Joseph Fourier Grenoble 1, CNRS/IN2P3, Institut National Polytechnique de Grenoble, Grenoble, France*
[l] *CPPM, Aix-Marseille Université, CNRS/IN2P3, Marseille, France*
[m] *LAL, Université Paris-Sud, CNRS/IN2P3, Orsay, France*
[n] *LPNHE, Universités Paris VI and VII, CNRS/IN2P3, Paris, France*
[o] *CEA, Irfu, SPP, Saclay, France*
[p] *IPHC, Université de Strasbourg, CNRS/IN2P3, Strasbourg, France*
[q] *IPNL, Université Lyon 1, CNRS/IN2P3, Villeurbanne, France*
[r] *Université de Lyon, Lyon, France*
[s] *III. Physikalisches Institut A, RWTH Aachen University, Aachen, Germany*
[t] *Physikalisches Institut, Universität Freiburg, Freiburg, Germany*
[u] *II. Physikalisches Institut, Georg-August-Universität Göttingen, Göttingen, Germany*
[v] *Institut für Physik, Universität Mainz, Mainz, Germany*
[w] *Ludwig-Maximilians-Universität München, München, Germany*
[x] *Panjab University, Chandigarh, India*
[y] *Delhi University, Delhi, India*
[z] *Tata Institute of Fundamental Research, Mumbai, India*
[aa] *University College Dublin, Dublin, Ireland*
[ab] *Korea Detector Laboratory, Korea University, Seoul, Republic of Korea*
[ac] *CINVESTAV, Mexico City, Mexico*
[ad] *Nikhef, Science Park, Amsterdam, The Netherlands*
[ae] *Radboud University Nijmegen, Nijmegen, The Netherlands*
[af] *Joint Institute for Nuclear Research, Dubna, Russia*
[ag] *Institute for Theoretical and Experimental Physics, Moscow, Russia*
[ah] *Moscow State University, Moscow, Russia*
[ai] *Institute for High Energy Physics, Protvino, Russia*
[aj] *Petersburg Nuclear Physics Institute, St. Petersburg, Russia*
[ak] *Institució Catalana de Recerca i Estudis Avançats (ICREA) and Institut de Física d'Altes Energies (IFAE), Barcelona, Spain*
[al] *Uppsala University, Uppsala, Sweden*
[am] *Taras Shevchenko National University of Kyiv, Kiev, Ukraine*
[an] *Lancaster University, Lancaster LA1 4YB, United Kingdom*
[ao] *Imperial College London, London SW7 2AZ, United Kingdom*
[ap] *The University of Manchester, Manchester M13 9PL, United Kingdom*
[aq] *University of Arizona, Tucson, AZ 85721, USA*

[ar] University of California Riverside, Riverside, CA 92521, USA
[as] Florida State University, Tallahassee, FL 32306, USA
[at] Fermi National Accelerator Laboratory, Batavia, IL 60510, USA
[au] University of Illinois at Chicago, Chicago, IL 60607, USA
[av] Northern Illinois University, DeKalb, IL 60115, USA
[aw] Northwestern University, Evanston, IL 60208, USA
[ax] Indiana University, Bloomington, IN 47405, USA
[ay] Purdue University Calumet, Hammond, IN 46323, USA
[az] University of Notre Dame, Notre Dame, IN 46556, USA
[ba] Iowa State University, Ames, IA 50011, USA
[bb] University of Kansas, Lawrence, KS 66045, USA
[bc] Louisiana Tech University, Ruston, LA 71272, USA
[bd] Northeastern University, Boston, MA 02115, USA
[be] University of Michigan, Ann Arbor, MI 48109, USA
[bf] Michigan State University, East Lansing, MI 48824, USA
[bg] University of Mississippi, University, MS 38677, USA
[bh] University of Nebraska, Lincoln, NE 68588, USA
[bi] Rutgers University, Piscataway, NJ 08855, USA
[bj] Princeton University, Princeton, NJ 08544, USA
[bk] State University of New York, Buffalo, NY 14260, USA
[bl] University of Rochester, Rochester, NY 14627, USA
[bm] State University of New York, Stony Brook, NY 11794, USA
[bn] Brookhaven National Laboratory, Upton, NY 11973, USA
[bo] Langston University, Langston, OK 73050, USA
[bp] University of Oklahoma, Norman, OK 73019, USA
[bq] Oklahoma State University, Stillwater, OK 74078, USA
[br] Brown University, Providence, RI 02912, USA
[bs] University of Texas, Arlington, TX 76019, USA
[bt] Southern Methodist University, Dallas, TX 75275, USA
[bu] Rice University, Houston, TX 77005, USA
[bv] University of Virginia, Charlottesville, VA 22904, USA
[bw] University of Washington, Seattle, WA 98195, USA

ARTICLE INFO

Article history:
Received 16 May 2014
Received in revised form 19 August 2014
Accepted 3 September 2014
Available online 8 September 2014
Editor: H. Weerts

ABSTRACT

We present the first measurements of the differential cross section $d\sigma/dp_T^\gamma$ for the production of an isolated photon in association with at least two b-quark jets. The measurements consider photons with rapidities $|y^\gamma| < 1.0$ and transverse momenta $30 < p_T^\gamma < 200$ GeV. The b-quark jets are required to have $p_T^{\text{jet}} > 15$ GeV and $|y^{\text{jet}}| < 1.5$. The ratio of differential production cross sections for $\gamma + 2$ b-jets to $\gamma + b$-jet as a function of p_T^γ is also presented. The results are based on the proton–antiproton collision data at $\sqrt{s} = 1.96$ TeV collected with the D0 detector at the Fermilab Tevatron Collider. The measured cross sections and their ratios are compared to the next-to-leading order perturbative QCD calculations as well as predictions based on the k_T-factorization approach and those from the SHERPA and PYTHIA Monte Carlo event generators.

In hadronic collisions, high-energy photons (γ) emerge unaltered from the hard parton–parton interaction and therefore provide a clean probe of the underlying hard-scattering dynamics [1]. Photons produced in these interactions (called direct or prompt) in association with one or more bottom (b)-quark jets provide an important test of perturbative Quantum Chromodynamics (QCD) predictions at large hard-scattering scales Q and over a wide range of parton momentum fractions. In addition, the study of these processes also provides information about the parton density functions (PDF) of b quarks and gluons (g), which still have substantial uncertainties. In $p\bar{p}$ collisions, $\gamma + b$-jet events are produced primarily through the Compton process $gb \to \gamma b$, which dominates for low and moderate photon transverse momenta (p_T^γ), and through quark–antiquark annihilation followed by $g \to b\bar{b}$ gluon splitting $q\bar{q} \to \gamma g \to \gamma b\bar{b}$, which dominates at high p_T^γ [2,3]. The final state with b-quark pair production, $p\bar{p} \to \gamma + b\bar{b}$, is mainly produced via $q\bar{q} \to \gamma b\bar{b}$ and $gg \to \gamma b\bar{b}$ scatterings [4]. The $\gamma + 2$ b-jet process is a crucial component of background in measurements of, for example, $t\bar{t}\gamma$ coupling [5] and in some searches for new phenomena. A series of measurements involving γ and $b(c)$-quark final states have previously been performed by the D0 and CDF Collaborations [3,6–9].

[1] Visitor from: Augustana College, Sioux Falls, SD, USA.
[2] Visitor from: The University of Liverpool, Liverpool, UK.
[3] Visitor from: DESY, Hamburg, Germany.
[4] Visitor from: Universidad Michoacana de San Nicolas de Hidalgo, Morelia, Mexico.
[5] Visitor from: SLAC, Menlo Park, CA, USA.
[6] Visitor from: University College London, London, UK.
[7] Visitor from: Centro de Investigacion en Computacion, IPN, Mexico City, Mexico.
[8] Visitor from: Universidade Estadual Paulista, São Paulo, Brazil.
[9] Visitor from: Karlsruher Institut für Technologie (KIT), Steinbuch Centre for Computing (SCC), D-76128 Karlsruhe, Germany.
[10] Visitor from: Office of Science, U.S. Department of Energy, Washington, DC 20585, USA.
[11] Visitor from: American Association for the Advancement of Science, Washington, DC 20005, USA.
[12] Visitor from: Kiev Institute for Nuclear Research, Kiev, Ukraine.
[13] Visitor from: University of Maryland, College Park, Maryland 20742, USA.

In this measurement, we follow an inclusive approach by allowing the final state with any additional jet(s) on top of the studied b-quark jets. Inclusive $\gamma + 2$ b-jet production may also originate from partonic subprocesses involving parton fragmentation into a photon. However, using photon isolation requirements significantly reduces the contributions from such processes. Next-to-leading order (NLO) calculations of the $\gamma + 2$ b-jet production cross section, which includes all b-quark mass effects, have recently become available [4]. These calculations are based on the four-flavor number scheme, which assumes four massless quark flavors and treats the b quark as a massive quark not appearing in the initial state.

This letter presents the first measurement of the cross section for associated production of an isolated photon with a bottom quark pair in $p\bar{p}$ collisions. The results are based on data corresponding to an integrated luminosity of 8.7 ± 0.5 fb^{-1} [10] collected with the D0 detector from June 2006 to September 2011 at the Fermilab Tevatron Collider at $\sqrt{s} = 1.96$ TeV. The large data sample and use of advanced photon and b-jet identification tools [11–13] enable us to measure the $\gamma + 2$ b-jet production cross section differentially as a function of p_T^γ for photons with rapidities $|y^\gamma| < 1.0$ and transverse momenta $30 < p_T^\gamma < 200$ GeV, while the b jets are required to have $p_T^{\text{jet}} > 15$ GeV and $|y^{\text{jet}}| < 1.5$. This allows for probing the dynamics of the production process over a wide kinematic range not studied before in other measurements of a vector boson $+b$-jet final state. The ratio of differential cross sections for $\gamma + 2$ b-jet production relative to $\gamma + b$-jet production is also presented in the same kinematic region and differentially in p_T^γ. The measurement of the ratio of cross sections leads to cancellation of various experimental and theoretical uncertainties, allowing a more precise comparison with the theoretical predictions.

The D0 detector is a general purpose detector described in detail elsewhere [14]. The subdetectors most relevant to this analysis are the central tracking system, composed of a silicon microstrip tracker (SMT) and a central fiber tracker embedded in a 1.9 T solenoidal magnetic field, the central preshower detector (CPS), and the calorimeter. The CPS is located immediately before the inner layer of the central calorimeter and is formed of approximately one radiation length of lead absorber followed by three layers of scintillating strips. The calorimeter consists of a central section (CC) with coverage in pseudorapidity of $|\eta_{\text{det}}| < 1.1$,[14] and two end calorimeters (EC) extending coverage to $|\eta_{\text{det}}| \approx 4.2$, each housed in a separate cryostat, with scintillators between the CC and EC cryostats providing sampling of developing showers for $1.1 < |\eta_{\text{det}}| < 1.4$. The electromagnetic (EM) section of the calorimeter is segmented longitudinally into four layers (EMi, $i = 1$–4), with transverse segmentation into cells of size $\Delta\eta_{\text{det}} \times \Delta\phi_{\text{det}} = 0.1 \times 0.1$ (see footnote 14), except EM3 (near the EM shower maximum), where it is 0.05×0.05. The calorimeter allows for a precise measurement of the energy of electrons and photons, providing an energy resolution of approximately 4% (3%) at an energy of 30 (100) GeV. The energy response of the calorimeter to photons is calibrated using electrons from Z boson decays. Because electrons and photons interact differently in the detector material before the calorimeter, additional energy corrections as a function of p_T^γ are derived using a detailed GEANT-based [15] simulation of the D0 detector response. These corrections are $\approx 2\%$ for photon candidates of $p_T^\gamma = 30$ GeV, and smaller for higher p_T^γ.

[14] The polar angle θ and the azimuthal angle ϕ are defined with respect to the positive z axis, which is along the proton beam direction. Pseudorapidity is defined as $\eta = -\ln[\tan(\theta/2)]$. Also, η_{det} and ϕ_{det} are the pseudorapidity and the azimuthal angle measured with respect, to the center of the detector.

The data used in this analysis are required to satisfy D0 experiment data quality criteria that ensure the proper functioning of detector subsystems (calorimeter and tracking detectors are most important for this analysis) [14] during data-taking. The data is collected using a combination of triggers requiring a cluster of energy in the EM calorimeter with loose shower shape requirements. The trigger efficiency is $\approx 96\%$ for photon candidates with $p_T^\gamma = 30$ GeV and 100% for $p_T^\gamma \gtrsim 40$ GeV. Offline event selection requires a reconstructed $p\bar{p}$ interaction vertex [16] within 60 cm of the center of the detector along the beam axis. The efficiency of the vertex requirement is $\approx$ (96–98)%, depending on p_T^γ. The missing transverse momentum in the event is required to be less than $0.7 p_T^\gamma$ to suppress background from $W \to e\nu$ decays. Such a requirement is highly efficient ($\geq 98\%$) for signal events.

Photon candidates are identified in the D0 detector as isolated clusters of energy deposits in the calorimeter with significant energy in the EM calorimeter layers and no spatially-matched track in the tracking system. The detailed description of photon selection and isolation criteria can be found in Refs. [3,6]. The photon selection efficiency and acceptance are calculated using samples of $\gamma + b$-jet events, generated with the SHERPA [17] and PYTHIA [18] Monte Carlo (MC) event generators. The samples are processed through a GEANT-based [15] simulation of the D0 detector. Simulated events are overlaid with data events from random $p\bar{p}$ crossings to properly model the effects of multiple $p\bar{p}$ interactions and noise in data. We ensure that the instantaneous luminosity distribution in the overlay events is similar to the data. The efficiency for photons to pass the identification criteria is (71–82)% with relative systematic uncertainty of 3%.

For the $\gamma + n$ b measurement ($n = 1, 2$), at least n jets with $p_T^{\text{jet}} > 15$ GeV and $|y^{\text{jet}}| < 1.5$ are selected. Jets are reconstructed using the D0 Run II algorithm [19] with a cone radius of $\mathcal{R} = 0.5$. A set of criteria is imposed to ensure that we have sufficient information to identify the jet as a heavy-flavor candidate: the jet is required to have at least two associated tracks with $p_T > 0.5$ GeV and at least one hit in the SMT, one of these tracks must also have $p_T > 1.0$ GeV. These criteria have an efficiency of about 90% for a b jet. Light jets (initiated by u, d and s quarks or gluons) are suppressed using a dedicated heavy-flavor (HF) tagging algorithm [13].

The HF tagging algorithm is based on a multivariate analysis (MVA) technique that combines information from the secondary vertex (SV) tagging algorithms and tracks impact parameter variables using an artificial neural network (NN) to define a single output discriminant, MVA_{bl} [13]. This algorithm utilizes the longer lifetimes of HF hadrons relative to their lighter counterparts. The MVA_{bl} has a continuous output value that tends towards one for b jet and zero for light jets. Events with at least two jets passing the $\text{MVA}_{\text{bl}} > 0.3$ selection are considered in the $\gamma + 2$ b-jet analysis. Depending on p_T^γ, this selection has an efficiency of (13–21)% for two b jets with relative systematic uncertainties of (4–6)%, primarily due to uncertainties on the data-to-MC correction factors [13]. Only (0.2–0.4)% of light-jets are misidentified as b jets.

After application of all selection requirements, 3816 $\gamma + 2$ b-jet candidate (186,406 $\gamma + b$-jet candidate) events remain in the data sample. In these events, there are two main background sources: jets misidentified as photons and light-flavor jets mimicking HF jets. To estimate the photon purity, the γ-NN distribution in data is fitted to a linear combination of templates for photons and jets obtained from simulated γ+jet and dijet samples. An independent fit is performed in each p_T^γ bin, yielding photon fractions between 62% and 90%, as shown in Fig. 1. The main systematic uncertainty in the photon fractions is due to the fragmentation model implemented in PYTHIA [20]. This uncertainty is estimated by varying the production rate of π^0 and η mesons by $\pm 50\%$ with respect to their

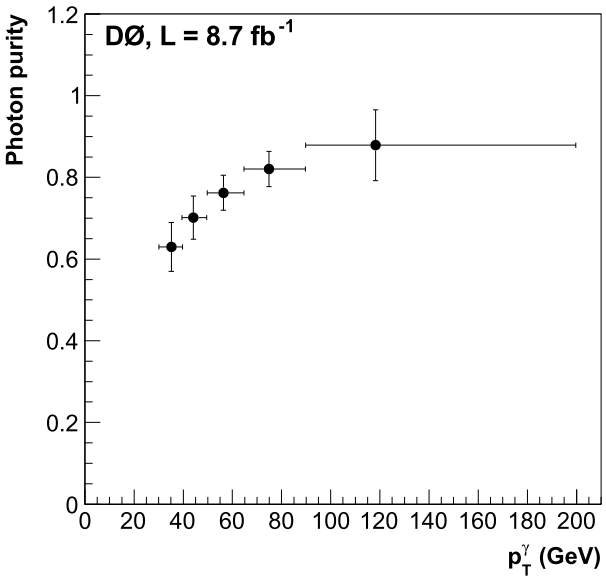

Fig. 1. Photon purity as a function of p_T^γ in the selected data sample. The error bars include statistical and systematic uncertainties added in quadrature. The binning is defined as in Table 1.

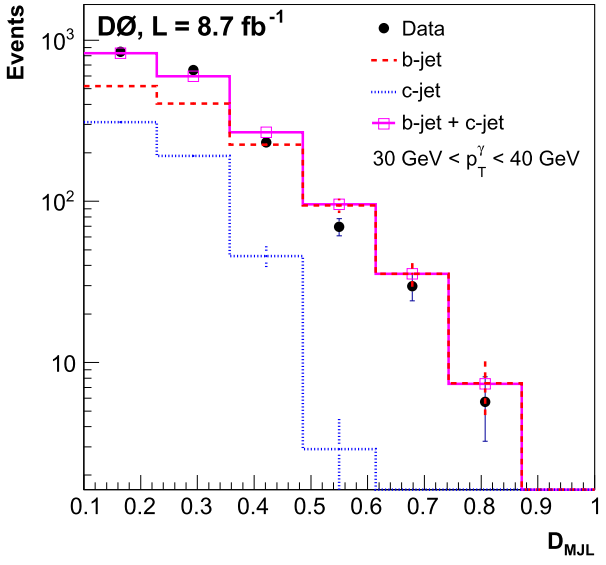

Fig. 2. (Color online.) Distribution of discriminant D_{MJL} after all selection criteria for a representative bin of $30 < p_T^\gamma < 40$ GeV. The expected contribution from the light jets component has been subtracted from the data. The distributions for the b-jet and c-jet templates (with statistical uncertainties) are shown normalized to their respective fitted fractions.

central values [21], and found to be about 6% at $p_T^\gamma \approx 30$ GeV, and $\leq 1\%$ at $p_T^\gamma \gtrsim 70$ GeV.

The fraction of different flavor jets in the selected data sample is extracted using a discriminant, D_{MJL}, with distributions dependent on the jet flavors. It combines two discriminating variables associated with the jet, mass of any secondary vertex associated with the jet M_{SV} and the probability for the jet tracks located within the jet cone to come from the primary $p\bar{p}$ interaction vertex. The latter probability is found using the jet lifetime impact parameter (JLIP) algorithm, and is denoted as P_{JLIP} [16]. The final D_{MJL} discriminant [22] is defined as $D_{\mathrm{MJL}} = 0.5 \times (M_{\mathrm{SV}}/5\ \mathrm{GeV} - \ln(P_{\mathrm{JLIP}})/20)$, where M_{SV} and $\ln(P_{\mathrm{JLIP}})$ are normalized by their maximum values obtained from the corresponding distributions in data. The data sample with two HF-tagged jets is fitted to templates consisting mainly of 2 b-jet and 2 c-jet events, as determined from MC simulation. The remaining jet flavor contributions in the sample (e.g., light + light-jets, light + $b(c)$-jets, etc.) are small and are subtracted from the data. The fractions of these rarer jet contributions are estimated from SHERPA simulation (which has been found to provide a good description of the data), and vary in the range (5–10)%. The difference in the values of these fractions obtained from SHERPA and PYTHIA, (2–4)%, is assigned as a systematic uncertainty on the background estimate. The fraction of 2 b-jet events are determined by performing a two-dimensional (corresponding to the 2 b-jet candidates) maximum likelihood fit of D_{MJL} distributions of 2 jet events in data using the corresponding templates for 2 b-jets and 2 c-jets. These jet flavor templates are obtained from MC simulations. As an example, the result of one of these maximum likelihood fits to D_{MJL} templates is presented in Fig. 2 (with $\chi^2/ndf = 6.80/5$ for data/MC agreement). This shows the one-dimensional projection onto the highest p_T jet D_{MJL} axis of the 2D fit, normalized to the number of events in data, for photons with $30 < p_T^\gamma < 40$ GeV. An independent fit is performed in each p_T^γ bin, resulting in extracted fractions of 2 b-jet events between 76% and 87%, as shown in Fig. 3. The relative uncertainties of the estimated 2 b-jet fractions range from 5% to 14%, increasing at higher p_T^γ and are dominated by the limited data statistics.

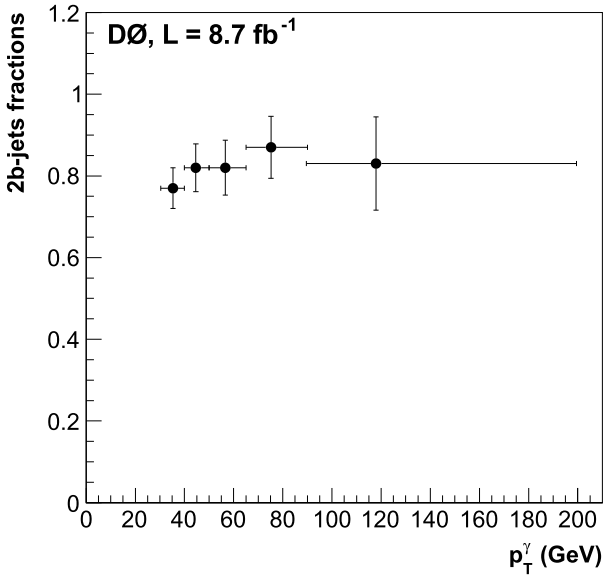

Fig. 3. The 2 b-jet fraction in data as a function of p_T^γ derived from the template fit to the heavy quark jet data sample after applying all selections. The error bars show both statistical and systematical uncertainties summed in quadrature. Binning is the same as given in Table 1.

By varying independently the requirements on photon and b-jet identification criteria from very loose to very tight selections, we find no evidence of a correlation between the measured photon purity and the 2 b-jet fraction. The obtained photon purity and 2 b-jet fractions are found to be consistent within uncertainties with the values determined using photon and b-jet identification criteria used with the default selections.

The estimated numbers of signal events in each p_T^γ bin are corrected for the geometric and kinematic acceptance of the photon and jets. The combined acceptance for photon and jets are calculated using SHERPA MC events. The acceptance is calculated for the photons satisfying $p_T^\gamma > 30$ GeV, $|y^\gamma| < 1.0$ at particle level. The particle level includes all stable particles as defined in Ref. [23]. The jets are required to have $p_T^{\mathrm{jet}} > 15$ GeV and $|y^{\mathrm{jet}}| < 1.5$. As in Refs. [3,6], in the acceptance calculations, the photon is required to be isolated by $E_T^{\mathrm{iso}} = E_T^{\mathrm{tot}}(0.4) - E_T^\gamma < 2.5$ GeV, where $E_T^{\mathrm{tot}}(0.4)$

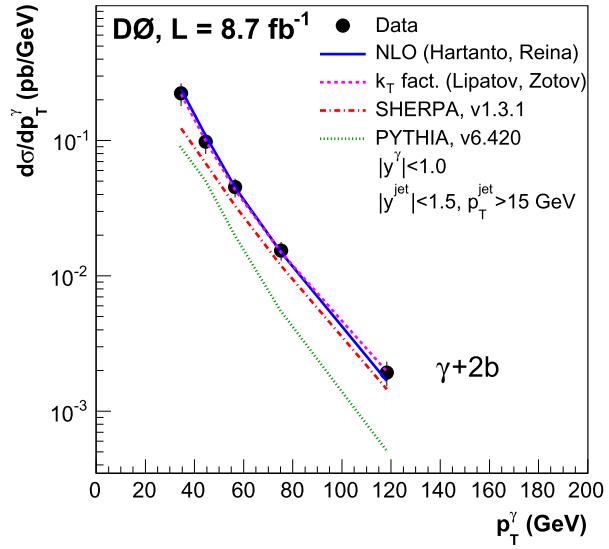

Fig. 4. (Color online.) The $\gamma+2$ b-jet differential production cross sections as a function of p_T^γ. The uncertainties on the data points include statistical and systematic contributions. The measurements are compared to the NLO QCD calculations [4] using the CT10nlo_nf4 PDFs [26] (solid line). The predictions from SHERPA [17], PYTHIA [18] and the k_T-factorization approach [29,30] are also shown.

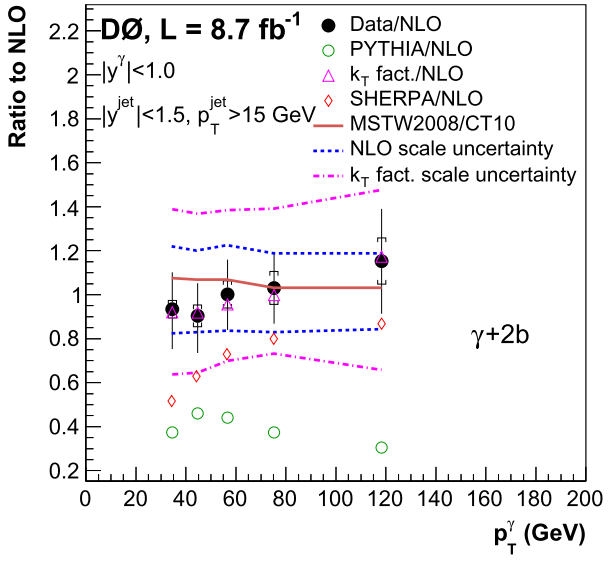

Fig. 5. (Color online.) The ratio of the measured $\gamma+2$ b-jet production cross sections to the reference NLO with CT10 predictions. The uncertainties on the data include both statistical (inner error bar) and total uncertainties (full error bar). Similar ratios to NLO calculations for predictions with SHERPA [17], PYTHIA [18] and k_T-factorization [29,30] are also presented along with the scale uncertainties on NLO and k_T-factorization predictions.

is the total transverse energy of particles within a cone of radius $\mathcal{R}=\sqrt{(\Delta\eta)^2+(\Delta\phi)^2}=0.4$ centered on the photon direction and E_T^γ is the photon transverse energy. The sum of transverse energy in the cone includes all stable particles [23]. The acceptance is driven by selection requirements in $|\eta_{\rm det}|$ (applied to avoid edge effects in the calorimeter regions used for the measurement) and $|\phi_{\rm det}|$ (to avoid periodic calorimeter module boundaries), photon $|\eta^\gamma|$ and p_T^γ, and bin-to-bin migration effects due to the finite energy resolution of the EM calorimeter. The combined photon and jets acceptance with respect to the p_T and rapidity selections varies between 66% and 77% in different p_T^γ bins. Uncertainties on the acceptance due to the jet energy scale [24], jet energy resolution, and the difference between results obtained with SHERPA and PYTHIA are in the range of (8–12)%.

The data, corrected for photon and jet acceptance, reconstruction efficiencies and the admixture of background events, are presented at the particle level by unfolding for effects of detector resolution, photon and b-jet detection inefficiencies. The differential cross sections of $\gamma+2$ b-jet production are extracted in five bins of p_T^γ. They are given in Table 1. The data points are plotted at the values of p_T^γ for which the value of a smooth function describing the dependence of the cross section on p_T^γ equals the averaged cross section in the bin [25].

The cross sections fall by more than two orders of magnitude in the range $30<p_T^\gamma<200$ GeV. The statistical uncertainty on the results ranges from 4.3% in the first p_T^γ bin to 9% in the last p_T^γ bin, while the total systematic uncertainty ranges up to 20%. Main sources of systematic uncertainty are the photon purity (up to 8%), photon and two b-jet acceptance (up to 14%), b-jet fraction (up to 13%), and integrated luminosity (6%) [10]. At higher p_T^γ, the uncertainty is dominated by the fractions of b-jet events and their selection efficiencies.

NLO perturbative QCD predictions, with the renormalization scale μ_R, factorization scale μ_F, and fragmentation scale μ_f all set to p_T^γ, are also given in Table 1. The uncertainty from the scale choice is (15–20)% and is estimated through a simultaneous variation of all three scales by a factor of two, i.e., for $\mu_{R,F,f}=0.5p_T^\gamma$ and $2p_T^\gamma$. The predictions utilize CT10nlo_nf4 PDFs [26] and are corrected for non-perturbative effects of parton-to-hadron fragmentation and multiple parton interactions. The latter are evaluated using SHERPA and PYTHIA MC samples with their standard settings [17,18]. The overall correction varies from about 0.90 at $30<p_T^\gamma<40$ GeV to about 0.95 at high p_T^γ, and an uncertainty of $\lesssim 2\%$ is assigned to account for differences between the two MC generators. NLO predictions based on MSTW2008 [27] are close to those made with NNPDF2.3 [28] and are slightly higher (up to 7% at small p_T^γ) than the predictions using CT10.

The predictions based on the k_T-factorization approach [29,30] and unintegrated parton distributions [31] are also given in Table 1. The k_T-factorization formalism contains additional contributions to the cross sections due to resummation of gluon radiation diagrams with k_T^2 above a scale μ^2 of $\mathcal{O}(1$ GeV), where k_T denotes the transverse momentum of the radiated gluon. Apart from this resummation, the non-vanishing transverse momentum distribution of the colliding partons are taken into account. These effects lead to a broadening of the photon transverse momentum distribution in this approach [29]. The scale uncertainties on these predictions vary from about 31% at $30<p_T^\gamma<40$ GeV to about 50% in the highest p_T^γ bin.

Table 1 also contains predictions from the PYTHIA [18] MC event generator with the CTEQ6.1L PDF set. It includes only $2\to 2$ matrix elements (ME) with $gb\to\gamma b$ and $q\bar{q}\to\gamma g$ scatterings (defined at LO) and with $g\to b\bar{b}$ splitting in the parton shower (PS). We also provide predictions of the SHERPA MC event generator [17] with the CTEQ6.6M PDF set [32]. For $\gamma+b$ production, SHERPA includes all the MEs with one photon and up to three jets, with at least one b-jet in our kinematic region. In particular, it accounts for an additional hard jet that accompanies the photon associated with 2 b jets. Compared to an NLO calculation, there is an additional benefit of imposing resummation (further emissions) through the consistent combination with the PS. Matching between the ME partons and the PS jets follows the prescription given in Ref. [33]. Systematic uncertainties are estimated by varying the ME-PS matching

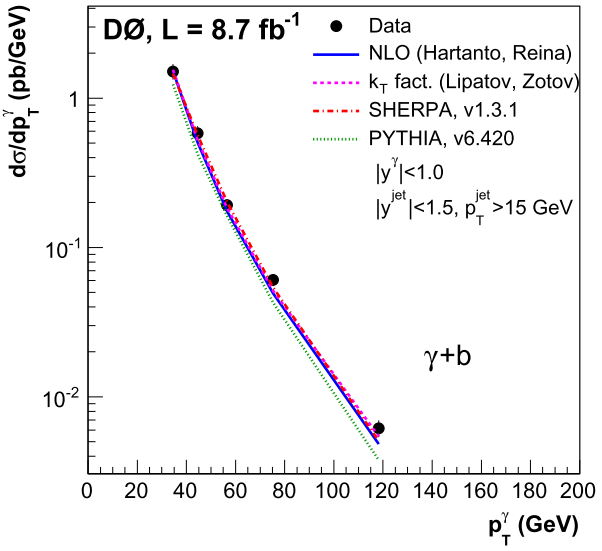

Fig. 6. (Color online.) The $\gamma + b$-jet differential production cross sections as a function of p_T^γ. The uncertainties on the data points include statistical and systematic contributions added in quadrature. The measurements are compared to the NLO QCD calculations [4] using the CTEQ6.6M PDFs [32] (solid line). The predictions from SHERPA [17], PYTHIA [18] and k_T-factorization [29,30] are also shown.

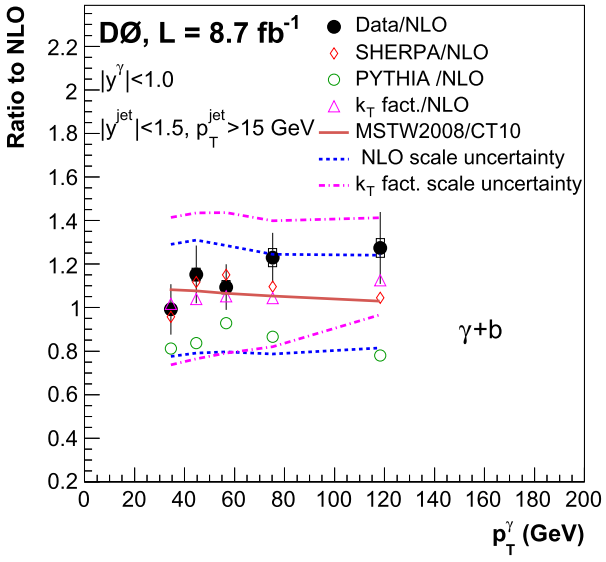

Fig. 7. (Color online.) The ratio of $\gamma + b$-jet production cross sections to NLO with CT10 predictions for data and theoretical predictions. The uncertainties on the data include both statistical (inner error bar) and total uncertainties (full error bar). The ratios to the NLO calculations with predictions from SHERPA [17], PYTHIA [18] and k_T-factorization [29,30] are also presented along with the scale uncertainties on NLO and k_T-factorization predictions.

scale by ± 5 GeV around the chosen central value.[15] As a result, the SHERPA cross sections vary up to $\pm 7\%$, the uncertainty being largest in the first p_T^γ bin.

All the theoretical predictions are obtained including the isolation requirement on the photon $E_T^{\rm iso} < 2.5$ GeV. The predictions are compared to data in Fig. 4 as a function of p_T^γ. The ratios of data to the NLO QCD calculations with CT10 and of different QCD predictions or MC simulation to the same NLO QCD calculations are shown in Fig. 5 as a function of p_T^γ.

The measured cross sections are well described by the NLO QCD calculations and the predictions from the k_T-factorization approach in the full studied p_T^γ region considering the experimental and theoretical uncertainties. Both of these predictions show consistent behavior, although the predictions from the k_T-factorization approach suffer from larger uncertainties. PYTHIA predicts significantly lower production rates and a more steeply falling p_T^γ distribution than observed in data. SHERPA performs better in describing the normalization at high p_T^γ, but underestimates production rates compared to that observed in data at low p_T^γ.

In addition to measuring the $\gamma + 2$ b-jet cross sections, we also obtain results for the inclusive $\gamma + b$-jet cross section in the same p_T^γ bins. Here we follow the same procedure as described in the previous similar D0 measurement [3]. However, as for the $\gamma + 2$ b-jet cross section measurement, we now use the most recent HF tagging algorithm [13]. The measured cross sections are shown in Fig. 6, and are compared to various predictions in Fig. 7. Data and predictions are also presented in Table 2. The values of the obtained $\gamma + b$-jet cross section are consistent with our previously published results [3].

We use $\sigma(\gamma + 2\ b\text{-jet})$ and $\sigma(\gamma + b\text{-jet})$ cross sections to calculate their ratio in bins of p_T^γ. Fig. 8 shows the p_T^γ spectrum of the measured ratio. The systematic uncertainties on the ratio vary within (11–15)%, being largest at high p_T^γ. The major sources of systematic uncertainties are attributed to the jet acceptances and the estimation of b-jet and 2 b-jet fractions obtained from the template fits to the data. Fig. 8 also shows comparisons with various predictions. The measurements are well described by the calculations done by NLO QCD and k_T-factorization predictions taking into account the experimental and theoretical uncertainties. The scale uncertainties on the NLO calculations are typically $\lesssim 15\%$, while they vary upto 35% at high p_T^γ for the k_T-factorization approach. The predictions from SHERPA describe the shape, but underestimate the ratio for most of the p_T^γ bins.

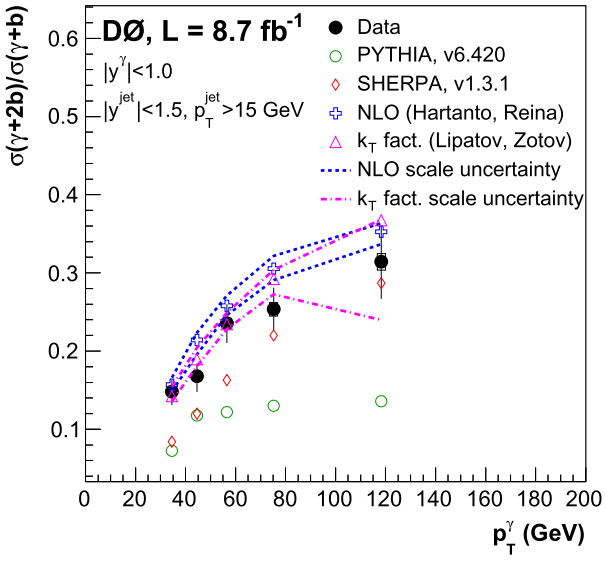

Fig. 8. (Color online.) The ratio of measured cross sections for $\gamma + 2$ b-jet to $\gamma + b$-jet production as a function of p_T^γ compared to theoretical predictions. The uncertainties on the data points include both statistical (inner error bar) and the full uncertainties (full error bar). The measurements are compared to the NLO QCD calculations [4]. The predictions from SHERPA [17], PYTHIA [18] and k_T-factorization [29, 30] are also shown along with the scale uncertainties on NLO and k_T-factorization predictions.

[15] We choose the following ME-PS matching parameters: the energy scale $Q_0 = 15$ GeV and the spatial scale $D = 0.4$, where D is taken to be of the radius of the photon isolation cone.

Table 1
The differential $\gamma + 2$ b-jet production cross sections $d\sigma/dp_T^\gamma$ in bins of p_T^γ for $|\eta^\gamma| < 1.0$, $p_T^{\text{jet}} > 15$ GeV and $|y^{\text{jet}}| < 1.5$ together with statistical uncertainties (δ_{stat}), total systematic uncertainties (δ_{syst}) and total uncertainties (δ_{tot}) which are obtained by adding δ_{stat} and δ_{syst} in quadrature. The last four columns show theoretical predictions obtained with NLO QCD, k_{T} factorization, and with the PYTHIA and the SHERPA event generators.

p_T^γ bin (GeV)	$\langle p_T^\gamma \rangle$ (GeV)	$d\sigma/dp_T^\gamma$ (pb/GeV)							
		Data	δ_{stat} (%)	δ_{syst} (%)	δ_{tot} (%)	NLO	k_{T} fact.	PYTHIA	SHERPA
30–40	34.5	2.24×10^{-1}	4.3	+19/−17	+19/−18	2.39×10^{-1}	2.20×10^{-1}	8.96×10^{-2}	1.23×10^{-1}
40–50	44.6	9.80×10^{-2}	5.4	+18/−15	+19/−16	1.08×10^{-1}	9.96×10^{-2}	4.99×10^{-2}	6.79×10^{-2}
50–65	56.6	4.52×10^{-2}	6.2	+15/−14	+16/−16	4.51×10^{-2}	4.31×10^{-2}	1.99×10^{-2}	3.29×10^{-2}
65–90	75.2	1.54×10^{-2}	7.2	+14/−14	+16/−16	1.49×10^{-2}	1.48×10^{-2}	5.57×10^{-3}	1.19×10^{-2}
90–200	118.3	1.93×10^{-3}	9.1	+19/−18	+21/−21	1.67×10^{-3}	1.96×10^{-3}	5.12×10^{-4}	1.45×10^{-3}

Table 2
The differential $\gamma + b$-jet production cross sections $d\sigma/dp_T^\gamma$ in bins of p_T^γ for $|\eta^\gamma| < 1.0$, $p_T^{\text{jet}} > 15$ GeV and $|y^{\text{jet}}| < 1.5$ together with statistical uncertainties (δ_{stat}), total systematic uncertainties (δ_{syst}), and total uncertainties (δ_{tot}) that are obtained by adding δ_{stat} and δ_{syst} in quadrature. The last four columns show theoretical predictions obtained with NLO QCD, k_{T}-factorization, and with the PYTHIA and the SHERPA event generators.

p_T^γ bin (GeV)	$\langle p_T^\gamma \rangle$ (GeV)	$d\sigma/dp_T^\gamma$ (pb/GeV)							
		Data	δ_{stat} (%)	δ_{syst} (%)	δ_{tot} (%)	NLO	k_{T} fact.	PYTHIA	SHERPA
30–40	34.5	1.51	2.3	12	12	1.52	1.69	1.23	1.46
40–50	44.6	5.83×10^{-1}	2.4	11	12	5.06×10^{-1}	5.70×10^{-1}	4.23×10^{-1}	5.65×10^{-1}
50–65	56.6	1.92×10^{-1}	2.8	9	10	1.75×10^{-1}	1.98×10^{-1}	1.63×10^{-1}	2.02×10^{-1}
65–90	75.2	6.06×10^{-2}	3.3	9	9	4.93×10^{-2}	5.43×10^{-2}	4.27×10^{-2}	5.41×10^{-2}
90–200	118.3	6.15×10^{-3}	3.3	13	13	4.83×10^{-3}	5.68×10^{-3}	3.76×10^{-3}	5.05×10^{-3}

Table 3
The $\sigma(\gamma + 2\ b\text{-jet})/\sigma(\gamma + b\text{-jet})$ cross section ratio in bins of p_T^γ for $|\eta^\gamma| < 1.0$, $p_T^{\text{jet}} > 15$ GeV and $|y^{\text{jet}}| < 1.5$ together with statistical uncertainties (δ_{stat}), total systematic uncertainties (δ_{syst}) and total uncertainties (δ_{tot}) which are obtained by adding δ_{stat} and δ_{syst} in quadrature. The last four columns show theoretical predictions obtained with NLO QCD, k_{T} factorization, and with the PYTHIA and the SHERPA event generators.

p_T^γ bin (GeV)	$\langle p_T^\gamma \rangle$ (GeV)	$\sigma(\gamma + 2\ b)/\sigma(\gamma + b)$							
		Data	δ_{stat} (%)	δ_{syst} (%)	δ_{tot} (%)	NLO	k_{T} fact.	PYTHIA	SHERPA
30–40	34.5	1.48×10^{-1}	2.3	+14/−6	+14/−6	1.58×10^{-1}	1.42×10^{-1}	7.25×10^{-2}	8.42×10^{-2}
40–50	44.6	1.68×10^{-1}	2.5	+13/−7	+13/−8	2.04×10^{-1}	1.89×10^{-1}	1.18×10^{-1}	1.20×10^{-1}
50–65	56.6	2.36×10^{-1}	2.8	+12/−8	+12/−8	2.59×10^{-1}	2.34×10^{-1}	1.22×10^{-1}	1.63×10^{-1}
65–90	75.2	2.54×10^{-1}	3.3	+11/−8	+12/−10	3.05×10^{-1}	2.92×10^{-1}	1.30×10^{-1}	2.20×10^{-1}
90–200	118.3	3.14×10^{-1}	3.4	+15/−14	+15/−15	3.52×10^{-1}	3.67×10^{-1}	1.36×10^{-1}	2.87×10^{-1}

The PYTHIA model does not perform well in describing the shape and underestimates ratios across all the bins. Experimental results as well as theoretical predictions for the ratios are presented in Table 3.

In summary, we have presented the first measurement of the differential cross section of inclusive production of a photon in association with two b-quark jets as a function of p_T^γ at the Fermilab Tevatron $p\bar{p}$ Collider. The results cover the kinematic range $30 < p_T^\gamma < 200$ GeV, $|y^\gamma| < 1.0$, $p_T^{\text{jet}} > 15$ GeV, and $|y^{\text{jet}}| < 1.5$. The measured cross sections are in agreement with the NLO QCD calculations and predictions from the k_T-factorization approach. We have also measured the ratio of differential $\sigma(\gamma + 2\ b\text{-jet})/\sigma(\gamma + b\text{-jet})$ in the same p_T^γ range. The ratio agrees with the predictions from NLO QCD and k_{T}-factorization approach within the theoretical and experimental uncertainties in the full studied p_T^γ range. These results can be used to further tune theory, MC event generators and improve the description of background processes in studies of the Higgs boson and searches for new phenomena beyond the Standard Model at the Tevatron and the LHC in final states involving the production of vector bosons in association with two b-quark jets.

Acknowledgements

We are grateful to the authors of the theoretical calculations, H.B. Hartanto, L. Reina, A. Lipatov and N. Zotov, for providing predictions and for many useful discussions.

We thank the staffs at Fermilab and collaborating institutions, and acknowledge support from the DOE and NSF (USA); CEA and CNRS/IN2P3 (France); MON, Rosatom and RFBR (Russia); CNPq, FAPERJ, FAPESP and FUNDUNESP (Brazil); DAE and DST (India); Colciencias (Colombia); CONACyT (Mexico); NRF (Korea); FOM (The Netherlands); STFC and the Royal Society (United Kingdom); MSMT and GACR (Czech Republic); BMBF and DFG (Germany); SFI (Ireland); The Swedish Research Council (Sweden); and CAS and CNSF (China).

References

[1] J.F. Owens, Rev. Mod. Phys. 59 (1987) 465.
[2] T. Stavreva, J.F. Owens, Phys. Rev. D 79 (2009) 054017.
[3] V.M. Abazov, et al., D0 Collaboration, Phys. Lett. B 714 (2012) 32.
[4] H.B. Hartanto, L. Reina, Phys. Rev. D 89 (2014) 074001.
[5] U. Baur, A. Juste, L. Orr, D. Rainwater, Phys. Rev. D 71 (2005) 054013.
[6] V.M. Abazov, et al., D0 Collaboration, Phys. Rev. Lett. 102 (2009) 192002.
[7] V.M. Abazov, et al., D0 Collaboration, Phys. Lett. B 719 (2013) 354.
[8] T. Aaltonen, et al., CDF Collaboration, Phys. Rev. D 81 (2010) 052006.
[9] T. Aaltonen, et al., CDF Collaboration, Phys. Rev. Lett. 111 (2013) 042003.
[10] T. Andeen, et al., 2007, FERMILAB-TM-2365.
[11] V.M. Abazov, et al., D0 Collaboration, Nucl. Instrum. Methods Phys. Res. A 750 (2014) 78.
[12] V.M. Abazov, et al., D0 Collaboration, Phys. Rev. Lett. 102 (2009) 231801.
[13] V.M. Abazov, et al., D0 Collaboration, Nucl. Instrum. Methods Phys. Res. A, submitted for publication, arXiv:1312.7623.
[14] V.M. Abazov, et al., D0 Collaboration, Nucl. Instrum. Methods Phys. Res. A 565 (2006) 463;
R. Angstadt, et al., Nucl. Instrum. Methods Phys. Res. A 622 (2010) 298;

M. Abolins, et al., Nucl. Instrum. Methods Phys. Res. A 584 (2008) 75.
[15] R. Brun, F. Carminati, CERN Program Library Long Writeup, W5013 (1993), we use geant version v3.21.
[16] V.M. Abazov, et al., D0 Collaboration, Nucl. Instrum. Methods Phys. Res. A 620 (2010) 490.
[17] T. Gleisberg, et al., J. High Energy Phys. 02 (2009) 007, we use sherpa version v1.3.1.
[18] T. Sjöstrand, S. Mrenna, P.Z. Skands, J. High Energy Phys. 05 (2006) 026, we use pythia version v6.420 with tune A.
[19] G.C. Blazey, et al., arXiv:hep-ex/0005012, 2000.
[20] V.M. Abazov, et al., D0 Collaboration, Phys. Lett. B 639 (2006) 151.
[21] T. Binoth, et al., Eur. Phys. J. C 4 (2002) 7.
[22] V.M. Abazov, et al., D0 Collaboration, Phys. Lett. B 718 (2013) 1314.
[23] C. Buttar, et al., arXiv:0803.0678 [hep-ph], Section 9.
[24] V.M. Abazov, et al., D0 Collaboration, Nucl. Instrum. Methods (2014), in press, arXiv:1312.6873.
[25] G.D. Lafferty, T.R. Wyatt, Nucl. Instrum. Methods Phys. Res. A 355 (1995) 541.
[26] H.-L. Lai, M. Guzzi, J. Huston, Z. Li, P.M. Nadolsky, J. Pumplin, C.-P. Yaun, Phys. Rev. D 82 (2010) 074024.
[27] A.D. Martin, et al., Eur. Phys. J. C 63 (2009) 189.
[28] R.D. Ball, et al., NNPDF Collaboration, Nucl. Phys. B 809 (2009) 1;
R.D. Ball, et al., NNPDF Collaboration, Nucl. Phys. B 816 (2009) 293, Erratum.
[29] A.V. Lipatov, N.P. Zotov, J. Phys. G 34 (2007) 219;
S.P. Baranov, A.V. Lipatov, N.P. Zotov, Eur. Phys. J. C 56 (2008) 371.
[30] A.V. Lipatov, N.P. Zotov, in preparation.
[31] M.A. Kimber, A.D. Martin, M.G. Ryskin, Phys. Rev. D 63 (2001) 114027.
[32] W.K. Tung, et al., J. High Energy Phys. 02 (2007) 052.
[33] A.D. Martin, W.J. Stirling, R.S. Thorne, G. Watt, Eur. Phys. J. C 63 (2009) 189.